A Mathematical Model for LPCVD in a Single Wafer Reactor

C. R. Kleijn, Th. H. van der Meer, and C. J. Hoogendoorn

Faculty of Applied Physics, Heat Transfer Section, Delft University of Technology, 2600 GA Delft, The Netherlands

ABSTRACT

A mathematical model for low-pressure chemical vapor deposition (LPCVD) in a single wafer reactor of the impinging jet type has been developed. The model includes the partial differential equations describing the balance of mass, momentum, heat, and species concentration, Stefan-Maxwell equations for multicomponent diffusion, multicomponent thermodiffusion, multiple surface reactions, and variable gas properties. Gas-phase chemistry is neglected. The equations are solved numerically in two-dimensional, axisymmetric form, using a control-volume-based finite difference method. The model is applied to silicon LPCVD from silane. It is shown that in single wafer LPCVD modeling, the coupling of the flow equations to the species concentrations is very important, as are thermodiffusion effects. Multicomponent diffusion phenomena can be modeled accurately using Wilke's approximation in many cases. In some situations, however, the Stefan-Maxwell equations should be used. The model is used to optimize both reactor geometry and process conditions, in order to obtain uniform deposition on large wafers at high growth rates. A series of parameter variations is presented, illustrating the power of the model as an aid in such an optimization study.

In the last two decades chemical vapor deposition (CVD) has become a dominating deposition technique in the integrated circuit industry. Numerous CVD reactors and processes have successfully been developed, *e.g.*, for the deposition of polysilicon, silicon dioxide and silicon nitride films, as well as metallic conductors such as tungsten and aluminum (1). Although the development of CVD techniques has been based largely on empirical findings and step-by-step improvement by methods of trial and error, the need for a more fundamental understanding of the relevant physicochemical mechanisms has been recognized in an early stage. The development of mathematical models, relating performance measures (*e.g.* deposition rate, film composition, and uniformity) to operating conditions (*e.g.*, pressure, reactant concentrations, gas flow, and reactor geometry) has played an important role in providing insight into the underlying chemical and physical processes.

The ideal CVD model would consist of a set of mathematical equations, describing all the relevant macroscopic CVD phenomena [gas flow, heat transfer, multicomponent (thermo)diffusion of reactants, carrier gases and reaction products, multi-step gas phase and surface chemistry, etc.], and relating these phenomena to both macroscopic and microscopic layer qualities. Although considerable progress has been made since the publication of the first simple analytical CVD models [*e.g.* by Shepherd (2) and Eversteijn, *et al.* (3)], none of the models that have been developed up to now incorporates all of these properties. Nevertheless, by attacking the problem of CVD modeling from many different angles, CVD models have led to an enormous increase in understanding of the important basic aspects of CVD processes.

Coltrin and co-workers (4, 5), for instance, made an extensive study of the complex gas phase chemistry in silicon CVD from silane, indicating the importance of gas phase reactions in CVD, especially at (near) atmospheric pressures. This model for the gas phase chemistry was found to give correct predictions of numerous experimental observations (6-8), making silicon CVD from silane the only CVD system up until now for which some basic understanding of the chemistry has really been obtained.

Using less rigorous models for the chemistry, other authors have focused their attention on the modeling of the gas flow and the transport of heat and species in several types of (near) atmospheric pressure CVD reactors, such as the classical horizontal reactors (9-11), barrel reactors (12), and different vertical reactor types. Thus a large number of experimentally observed phenomena have been predicted successfully by mathematical models of increasing complexity. Probably the most complete model for atmospheric pressure CVD is the model for silicon CVD by Moffat and Jensen (13), incorporating three-dimensional transport phenomena as well as rather detailed gas phase and surface chemistry.

A third direction in which CVD modeling has made considerable progress is the modeling of low-pressure CVD (LPCVD) in so-called boat reactors, carried out at pressures of typically 0.1-1 torr. Although an accurate description of these LPCVD processes demands less sophisticated modeling of the gas flow and gas phase chemistry, these two being obviously of relatively small importance in LPCVD, other aspects such as multicomponent diffusion, multireaction schemes, varying gas properties due to large concentration differences and, for very low pressures, deviations from continuum theory due to large Knudsen numbers, demand special care in this type of modeling. By inclusion of these effects into a numerical model Jensen and Graves (14) and Roenigk and Jensen (15) could successfully describe the deposition of (*in situ* doped) polysilicon in a LPCVD boat reactor.

An extensive review of CVD modeling has been given by Hess *et al.* (16) and Jensen (17). In these reviews it is concluded that CVD modeling up to now can be appropriately handled in terms of LPCVD in boat reactors, with multicomponent reaction-diffusion effects dominating the process, and cold wall, near-atmospheric pressure reactors, in which fluid flow and gas phase reactions are also important. The main bottleneck in CVD modeling at the moment seems to be the insufficient knowledge of the chemistry involved. Mathematical models for CVD, in combination with appropriate experiments in real reactors, may lead to a further understanding of CVD chemistry.

However, it is now widely felt (16-18), that the conventional types of reactors that have been the subject of CVD modeling up to now are not very suitable for this purpose. For instance, the complex entrance effects and largely unknown thermal boundary conditions have been a major drawback in obtaining accurate predictions of the deposition in horizontal CVD reactors (11). It has therefore been stated that efforts to unravel the basic concepts of CVD would greatly be aided by a judicious choice of reactor configuration. By developing reactors with a well defined flow field, thermal boundary conditions, etc., and coupling modeling results for these reactors to specially designed experiments, important progress in CVD modeling is expected to be possible. For this purpose, reactors of the rotating disk, impinging jet, and stagnation point flow type have been suggested (16-18). This has led to an increasing effort in the development of mathematical models for reactors of one of these three types.

Pollard and Newman (19) made a one-dimensional model for CVD in a rotating disk reactor, including gas phase and surface reactions as well as multicomponent diffusion. However, phenomena such as boundary effects at the edge of the disk and natural convection cannot be included in a one-dimensional model. Therefore, Evans and Greif (20, 21) made a two-dimensional analysis of the problem, investigating the effects of buoyancy and boundaries on the local Nusselt numbers on the disk, as compared to the one-dimensional case. Wahl (22, 23) studied CVD processes in stagnation point flow. Using a two-dimensional axisymmetric model, including mixed convection and thermodiffusion, experimental results on deposition profiles could be calculated using one fitting parameter.

Houtman *et al.* (24) compared two-dimensional modeling results to the classical one-dimensional treatment of stagnation point flow, thus giving an overview of the parameter ranges for which the 1-D treatment will give reasonably accurate results. Lee *et al.* (25) compared modeling results for MOCVD in an inverted stagnation point flow to experimentally observed growth rates. The impinging jet configuration has been studied by Michaelidis and Pollard (26) and Jenkinson and Pollard (27). For these studies a one-dimensional model, including multicomponent diffusion, thermodiffusion, and gas phase and surface chemistry, was used.

At the same time, with increasing wafer dimensions in the commercial IC industry, the interest in single-wafer LPCVD reactors has grown considerably (1). As a basic concept for these reactors, again, the main interest is in impinging jet, rotating disk, and stagnation point flow configurations. Besides other advantages over conventional batch-type LPCVD reactors, such as low price, easy automatic wafer handling and small floor area in the clean room, the most important advantage of single wafer reactors is the possibility of obtaining excellent deposition uniformity over large wafers at high growth rates. To obtain sufficient throughput, both pressure and temperature in single wafer LPCVD will have to be increased compared to conventional LPCVD. To prevent deposition on the walls, these will usually be cooled in single wafer reactors.

From the above it is clear that the combined experimental and modeling research of low pressure single wafer reactors, *e.g.*, of the impinging jet type, is of great importance, from a fundamental scientific as well as from an IC industry-oriented point of view. However, most modeling for impinging jet type reactors has been devoted to atmospheric pressure CVD, with mass-transfer limited deposition, highly diluted reactants, and important gas phase chemistry. In single wafer LPCVD, on the other hand, reactants will usually be much less diluted, deposition will be kinetically limited, and gas phase reactions will be relatively unimportant compared to surface reactions. This requires that different mathematical models be used. As far as modeling is concerned, the single wafer LPCVD reactor combines some of the aspects of LPCVD boat reactors and atmospheric pressure cold wall systems. In single wafer LPCVD, complex gas flow phenomena, including buoyancy effects and thermodiffusion, will be important. At the same time, multicomponent diffusion effects and strong coupling between gas flow and concentration field will play an important role, as in conventional LPCVD. The combination of these phenomena invalidates some simplifying assumptions commonly made in CVD modeling.

It is the purpose of this paper to discuss the development of a mathematical model for a single wafer LPCVD reactor of the impinging jet type, incorporating all these phenomena, and to illustrate the possibilities of such a model in reactor design and process optimization. Special attention will be given to some modeling aspects typical for single wafer LPCVD. Although the present model is not restricted to a specific process, the deposition of polysilicon from silane is chosen as an illustration, mainly because of the relatively well-known chemistry for this process. Comparison of modeling results with growth experiments and diagnostic experiments in a specially built research reactor, similar to the one studied in this paper, will be the subject of forthcoming publications.

Mathematical Model

The mathematical model developed for LPCVD in a single wafer reactor consists of a set of partial differential equations with appropriate boundary conditions, describing the gas flow and the transport of energy and species, as well as relations for the transport properties as a function of temperature, pressure, and mixture composition. Some simplifying assumptions will generally apply to CVD systems.

First, stationary, laminar gas flow is assumed. Reynolds numbers in CVD systems will usually be of the order 1-100, *i.e.*, far below values at which the onset of turbulence might be expected [$\simeq 2 \cdot 10^3$ (28)]. Rayleigh numbers in low pressure (0.1-10 torr) CVD systems are typically of the order 10^{-3}-$2 \cdot 10^3$ for nitrogen as a carrier gas, whereas for hydrogen these values will be 50 times lower. Unsteady motion in a horizontal gas layer heated from below will develop at Rayleigh numbers $>6 \cdot 10^3$, whereas transition to turbulent motion occurs at Rayleigh numbers $>3 \cdot 10^4$ (29). A superimposed forced convection flow as in CVD has a stabilizing effect, delaying the transition to unsteady and turbulent motion to even higher Rayleigh numbers (30).

Secondly, a steady-state situation is considered. This is allowed when the time scales associated with transient effects during deposition (such as the disturbance of the temperature field in the reactor due to the introduction of the wafer and unsteadiness in the concentration field at the onset and offset of the reactants supply) are small compared to the total deposition time. The latter will be 5-10 min in a single wafer reactor.

Thirdly, ideal gases are assumed, as well as the validity of the continuum approach. The latter becomes dubious at very low pressures ($\simeq$0.1 torr), where mean free path lengths of the molecules will be a few mm. However, at pressures of 1-10 torr, common in single wafer LPCVD, the continuum approach will be valid. The three assumptions above and several minor ones stated below reduce the general transport equations to the following forms.

Equations describing the flow and temperature field.— The mean gas flow in the reactor is described by the momentum balance equation or Navier Stokes equation and the continuity equation, which are coupled to the energy equation due to buoyancy effects. For stationary flow the continuity equation becomes

$$\nabla \cdot (\rho \mathbf{v}) = 0 \qquad [1]$$

The Navier Stokes equation can be written as

$$\nabla \cdot (\rho \mathbf{v}\mathbf{v}) = \nabla \cdot \boldsymbol{\tau} - \nabla P + \rho \mathbf{g} \qquad [2]$$

where the viscous stress tensor $\boldsymbol{\tau}$ takes the form

$$\boldsymbol{\tau} = \mu (\nabla \mathbf{v} + (\nabla \mathbf{v})^T) + (\kappa - \frac{2}{3}\mu)(\nabla \cdot \mathbf{v}) \cdot \mathbf{I} \qquad [3]$$

assuming that the gas mixture will behave as a Newtonian fluid.

In the energy equation, describing the temperature field in the reactor, we may well neglect viscous dissipation (31) and Dufour effects (27). Because of the low pressures, the emission and absorption of radiation by the gases may also be neglected. Also, at these low Mach number flows, pressure effects are negligible. Furthermore, we will assume that at these low pressures gas phase reactions are negligible, thus eliminating the need to include the heat of reaction in the energy equation. We now get

$$c_p \nabla \cdot (\rho \mathbf{v} T) = \nabla \cdot (\lambda \nabla T) \qquad [4]$$

In the above equations, the fluid properties λ, μ, ρ and c_p are not only functions of temperature and pressure, but also of the composition of the gas mixture. Thus, the energy and flow equations given above will be coupled to the species balance equations.

Species balance equations.—When neglecting gas phase reactions, the balance equations for gas species i can be written as

$$\nabla \cdot (\rho \mathbf{v} \omega_i) = -\nabla \cdot \mathbf{j}_i \qquad [5]$$

in which the total diffusive mass flux $\mathbf{j}_i$ of species i is composed of diffusion fluxes due to concentration gradients and diffusion fluxes due to thermal diffusion

$$\mathbf{j}_i = \mathbf{j}_i^C + \mathbf{j}_i^T \qquad [6]$$

In an N-component gas mixture there will be N-1 independent species equations of the form of Eq. [5], since the mass fractions must sum up to 1

$$\sum_i \omega_i = 1 \qquad [7]$$

Note that the species balance equations are written in terms of mass fractions ω_i and mass fluxes $\mathbf{j}_i$, instead of the commonly used mole fractions and fluxes. In the latter approach the mole-averaged velocity is needed, whereas from the Navier Stokes equations the mass-averaged velocity is obtained. Therefore, in case of coupled species and flow equations, the first approach is preferable.

A general expression for the diffusion fluxes $\mathbf{j}_i^c$ due to concentration gradients in a multicomponent gas mixture is given by the Stefan-Maxwell equations, usually written in terms of mole fractions and fluxes (31)

$$\nabla x_i = \sum_{j \neq i} \frac{1}{cD_{ij}} (x_i \mathbf{J}_j^C - \mathbf{x}_j \mathbf{J}_i^C) \quad [8]$$

In terms of mass fractions and fluxes we obtain

$$\nabla \omega_i + \omega_i \nabla (\ln m) = \sum_{j \neq i} \frac{1}{\rho D_{ij}} \left(\frac{m\omega_i}{m_j} \cdot \mathbf{j}_j^C - \frac{m\omega_j}{m_j} \cdot \mathbf{j}_i^C \right) \quad [9]$$

Again, in an N-component gas mixture there are N-1 independent equations of the form of Eq. [9]. Together with the additional equation

$$\sum_i \mathbf{j}_i^C = 0 \quad [10]$$

they form a closed set of equations from which the N diffusive mass fluxes $\mathbf{j}_i^C$ can be solved. From Eq. [9] we can derive an explicit expression for $\mathbf{j}_i^C$, assuming that all the other fluxes $\mathbf{j}_j^C$ are known

$$\mathbf{j}_i^C = -\rho \mathbb{D}_i \nabla \omega_i - \rho \omega_i \mathbb{D}_i \nabla (\ln m) + m\omega_i \mathbb{D}_i \sum_{j \neq i} \frac{\mathbf{j}_j^C}{m_j D_{ij}} \quad [11]$$

with $\mathbb{D}_i$ an effective diffusion coefficient for species i

$$\mathbb{D}_i = \left(\sum_{j \neq i} \frac{m\omega_j}{m_j D_{ij}} \right)^{-1} \quad [12]$$

The above expressions [11] and [12] can be used to solve the set of Stefan-Maxwell equations iteratively.

As an alternative to the Stefan-Maxwell equations, an approximate expression for the diffusive fluxes in a multicomponent gas mixture has been derived by Wilke (32). Here the diffusion of species i in a multicomponent mixture is written in the form of Fick's law of diffusion with an effective diffusion coefficient $\mathbb{D}'_i$ instead of the binary diffusion coefficient

$$\mathbf{j}_i^C = -\rho \mathbb{D}'_i \nabla \omega_i \quad [13]$$

with

$$\mathbb{D}'_i = \left(1 - \frac{m\omega_i}{m_i} \right) \cdot \left(\sum_{j \neq i} \frac{m\omega_j}{m_j D_{ij}} \right)^{-1} \quad [14]$$

In the case of a highly diluted species ($\omega_i << 1$), the full Stefan-Maxwell equations and Wilke's approximation are identical. For binary mixtures ($N = 2$) both approaches lead to Fick's law of diffusion. When Wilke's approximation is used to calculate the diffusive fluxes in a multicomponent mixture, the N equations of the form of Eq. [13] form an independent set, which is not consistent with Eq. [10]. Therefore, in order to be able to fulfill Eq. [10], one of the equations must be dropped. Wilke's approximation to the full Stefan-Maxwell equations, as well as other approximations, have been discussed by Coffee and Heimerl (33).

The diffusive mass fluxes due to thermodiffusion (Soret effect) are given by

$$\mathbf{j}_i^T = -\mathbb{D}_i^T \nabla (\ln T) \quad [15]$$

in which $\mathbb{D}_i^T$ is the multicomponent thermodiffusion coefficient for species i. Thermodiffusion will cause a concentration of large, heavy molecules in cold regions, whereas small, light molecules will move towards the hot regions. The thermodiffusion fluxes for all species sum up to zero.

Table I. Fitting relations for the transport properties

$\mu = c_0 + c_1 \cdot T + c_2 \cdot T^2$
$\lambda = c_0 + c_1 \cdot T + c_2 \cdot T^2$
$c_p = c_0 + c_1 \cdot T + c_2 \cdot T^2$
$D_{12} = (c_0 + c_1 \cdot T + c_2 \cdot T^2)/P$
$D_{21} = D_{12}$

Property	Gas (pair)	c_0	c_1	c_2
μ	SiH_4	$1.47 \cdot 10^{-6}$	$3.66 \cdot 10^{-8}$	$-6.81 \cdot 10^{-12}$
	N_2	$5.73 \cdot 10^{-6}$	$4.37 \cdot 10^{-8}$	$-9.28 \cdot 10^{-12}$
	H_2	$3.11 \cdot 10^{-6}$	$2.06 \cdot 10^{-8}$	$-3.54 \cdot 10^{-12}$
λ	SiH_4	$-2.12 \cdot 10^{-2}$	$1.45 \cdot 10^{-4}$	$-1.31 \cdot 10^{-8}$
	N_2	$8.54 \cdot 10^{-3}$	$6.23 \cdot 10^{-5}$	$-4.34 \cdot 10^{-9}$
	H_2	$1.05 \cdot 10^{-1}$	$3.21 \cdot 10^{-4}$	$-2.50 \cdot 10^{-9}$
c_p	SiH_4	$4.74 \cdot 10^{2}$	$3.26 \cdot 10^{0}$	$-1.08 \cdot 10^{-3}$
	N_2	$9.83 \cdot 10^{2}$	$1.58 \cdot 10^{-1}$	$1.69 \cdot 10^{-5}$
	H_2	$1.47 \cdot 10^{4}$	$-1.01 \cdot 10^{0}$	$1.29 \cdot 10^{-3}$
D_{12}	SiH_4, N_2	$-9.64 \cdot 10^{-1}$	$6.25 \cdot 10^{-3}$	$8.50 \cdot 10^{-6}$
	SiH_4, H_2	$-2.90 \cdot 10^{0}$	$2.06 \cdot 10^{-2}$	$2.81 \cdot 10^{-5}$
	N_2, H_2	$-3.20 \cdot 10^{0}$	$2.44 \cdot 10^{-2}$	$3.37 \cdot 10^{-5}$

Transport properties of gas species and mixtures.—In the above equations several transport properties appear, which will in general be a function of temperature, pressure and mixture composition. To compute their values, the transport properties of the constituent species as a function of temperature and pressure must be known. Values for the specific heats of the species were taken from Svehla (34). The bulk viscosity was neglected (31). The viscosities, thermal conductivities, and binary diffusion coefficients can be obtained from statistical mechanical calculations (34, 35) or, when available, from experimental data (36-38). Second-order polynomials were used to fit their temperature dependence (Table I). The density and specific heat of the mixture may now be calculated straightforward from

$$\rho = \frac{Pm}{RT} \quad [16]$$

with

$$m = \sum_i x_i m_i \quad [17]$$

and

$$c_p = \sum_i \omega_i c_{pi} \quad [18]$$

Several methods for calculating the viscosity and thermal conductivity of a gas mixture have been evaluated by Bretsznajder (39). Following his recommendations, the following relations were used

$$\mu = \sum_i \left(\frac{x_i \mu_i}{\sum_j x_j \Phi_{ij}} \right) \quad [19]$$

with

$$\Phi_{ij} = \frac{1}{\sqrt{8}} \left(1 + \frac{m_i}{m_j} \right)^{-1/2} \cdot \left(1 + \left(\frac{\mu_i}{\mu_j} \right)^{1/2} \cdot \left(\frac{m_j}{m_i} \right)^{1/4} \right)^2 \quad [20]$$

and

$$\lambda = \alpha \sum_i \lambda_i x_i + (1 - \alpha) \cdot \left(\sum_i \frac{x_i}{\lambda_i} \right)^{-1} \quad [21]$$

in which α is a fraction ($0.32 \leq \alpha \leq 0.80$), the value of which depends on the mole fraction of light gases (He, H_2) in the mixture.

Table II. Fitting relations for binary thermodiffusion ratios

$k_{12} = c_0 x_1 x_2 \cdot (1 + c_1 x_1 + c_2 x_1^2 + c_3 x_1^3) \cdot (1 + c_4 \exp(c_5 T))$
$k_{21} = -k_{12}$

Gas pair	c_0	c_1	c_2	c_3	c_4	c_5
N_2, SiH_4	−0.0515	0.186	0.0294	0.00443	−1.69	−0.00494
H_2, N_2	−0.271	0.727	−0.357	0.987	−1.61	−0.00915
H_2, SiH_4	−0.274	1.01	−1.04	1.90	−1.70	−0.00635

The binary thermodiffusion coefficient may be calculated from

$$D_{12}^T = \frac{c^2}{\rho} m_1 m_2 D_{12} k_{12} \quad [22]$$

where k_{12} is the thermodiffusion ratio, which may be obtained from statistical mechanical calculations (35). Unlike other transport properties, the thermodiffusion ratio is very sensitive to the assumed intermolecular potential energy function. When the Lennard-Jones (6-12) potential is used, k_{12} for a given gas pair is a function of temperature and composition

$$k_{12} = k_{12}(x_1, x_2, T) \quad [23]$$

This dependence was fitted using the product of a third-order polynomial in x_1 and an expotential function in T (Table II). Using the binary thermodiffusion coefficients, an approximate approach, suggested by Clark Jones (40), was used to calculate the multicomponent thermodiffusion coefficients. In view of the relative inaccuracy associated with the calculation of thermodiffusion coefficients and the fact that thermodiffusion is only a second-order effect compared to ordinary diffusion in CVD, the computational complexity of the exact formulation for multicomponent thermodiffusion coefficients (35) does not seem justified. Thus we used

$$\mathbb{D}_i^T = \sum_{j \neq i} \frac{c^2}{\rho} m_i m_j D_{ij} k_{ij} \quad [24]$$

which should be compared to Eq. [22]. The above approximation is exact for multicomponent mixtures of isotopes and for binary mixtures. Furthermore, this approach ensures that the sum of all thermodiffusion mass fluxes $\mathbf{j}_i^T$ equals zero, as it should.

Boundary conditions.—To make the above set of equations a well-posed problem, boundary conditions must be specified for the velocity components, the temperature, and the species concentrations. Furthermore, the pressure must be specified at one particular point. In Fig. 1 a representation of the modeled single wafer LPCVD reactor is given. The reactor is axisymmetric, so no variations or velocities in the angular direction were assumed. Boundary conditions must be specified at the inlet, outlet, solid walls, symmetry axis, and wafer surface. They are all indicated in Fig. 2 and are rather straightforward, except perhaps for the boundary conditions at the wafer surface. At the wafer surface K surface reactions will take place of the form

$$\gamma_{1k}G_1 + \gamma_{2k}G_2 + \ldots \rightarrow \gamma_{nk}G_n + \gamma_{n+1k}G_{n+1} + \ldots + \sigma_{1k}S_1 + \sigma_{2k}S_2 + \ldots \quad [25]$$

with G_i the gaseous reactants and reaction products ($i = 1, N$), S_j the solid reaction products ($j = 1, S$) and γ_{ik} and σ_{jk} ($k = 1, K$) the stoichiometric coefficients, which are positive for products and negative for reactants. Due to these surface reactions there will be a net mass production rate of gaseous species i at the wafer surface

$$M_i = \sum_k \gamma_{ik} R_k m_i \quad [26]$$

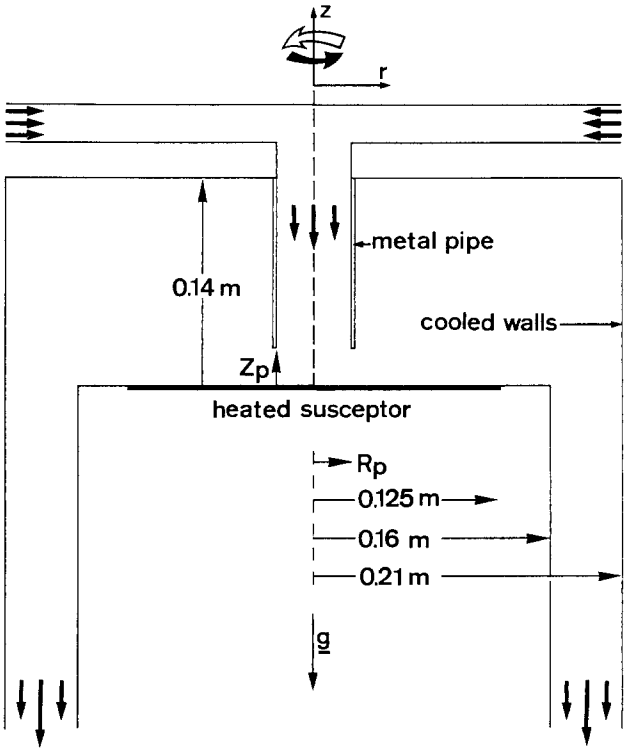

Fig. 1. Schematic representation of the modeled single wafer LPCVD reactor. R_p is the radius of the inflow pipe, Z_p is the axial distance from the wafer to the end of the inflow pipe.

and the total net mass flux normal to the wafer surface will be

$$M = \sum_i \sum_k \gamma_{ik} R_k m_i \quad [27]$$

leading to a velocity component normal to the wafer surface

$$v_z \text{ (wafer surface)} = -\frac{1}{\rho} \sum_i \sum_k \gamma_{ik} R_k m_i \quad [28]$$

The pressure is prescribed in the outlet of the reactor.

Chemical model.—The mathematical model described in the previous section is not restricted to any particular LPCVD process. The composition of the reacting gas mixture and the set of surface reactions can be chosen freely in order to model different processes. The only restriction in the model is the assumption that gas phase reactions are negligible, thus restricting the model to low pressure CVD.

In this paper, the model is applied to LPCVD of silicon from silane. A simple model for the chemistry was used, assuming that gas phase reactions are negligible at these low pressures and that deposition is due to the surface adsorption of silane followed by the decomposition of silane into silicon and hydrogen, leading to one overall surface reaction (41, 42)

$$SiH_4(g) \rightarrow Si(s) + 2H_2(g) \quad [29]$$

When the surface adsorption of silane is considered rate-limiting a deposition rate

$$R = \frac{k \cdot P_{SiH_4}}{1 + K_H (P_{H_2})^{1/2} + K_S P_{SiH_4}} \quad [30]$$

is found. Following Roenigk and Jensen (15), who successfully used the above chemical model to predict deposition rates for silicon LPCVD from silane in a boat reactor, the following values for the constants appearing in Eq. [30] were used

k = $1.6 \cdot 10^4 \exp(-18{,}500/T)$ mole $\cdot m^{-2} \cdot s^{-1} \cdot Pa^{-1}$
K_H = 0.19 $Pa^{-1/2}$
K_S = 0.70 Pa^{-1}

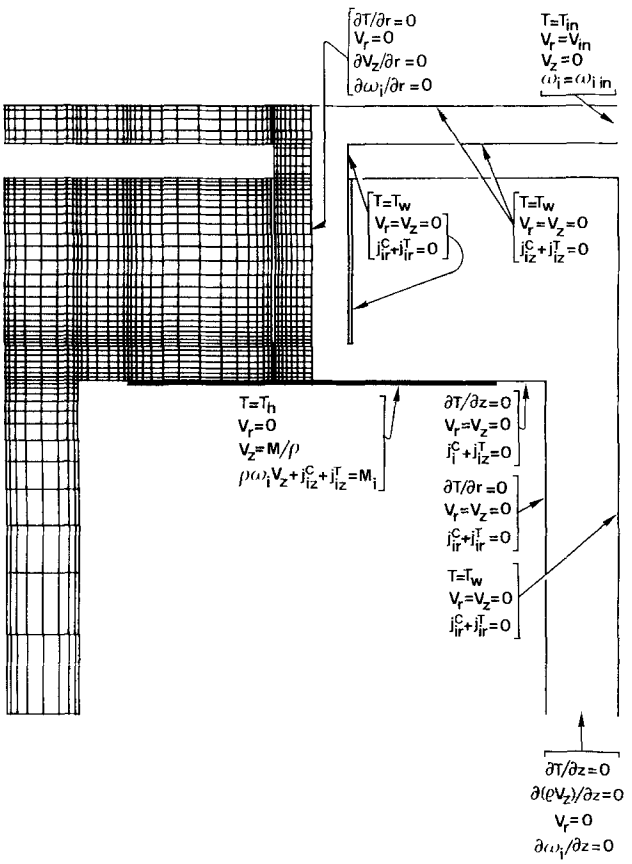

Fig. 2. Computational grid and boundary conditions

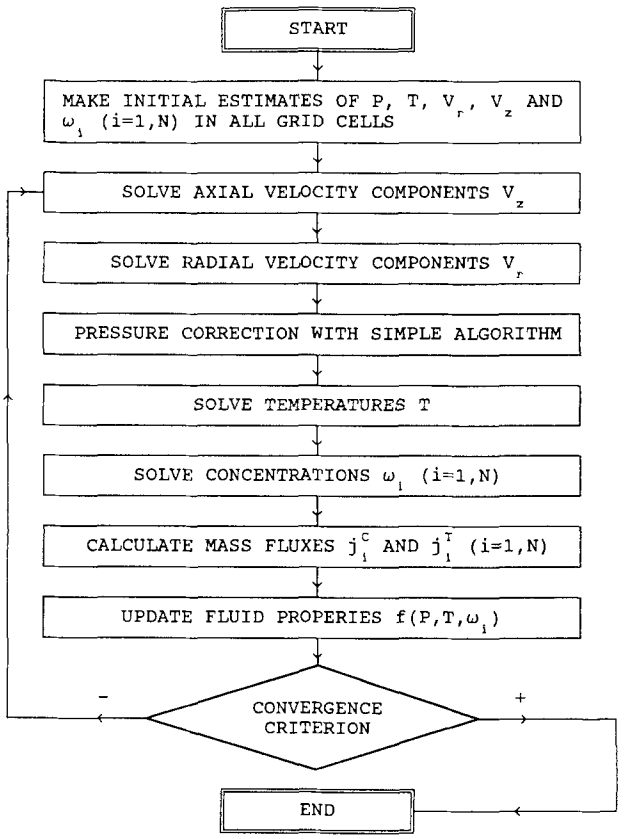

Fig. 3. Schematic representation of the numercial solution procedure

Using this chemical model, the total number of gaseous species N in the system will be 2 or 3 (silane, hydrogen, and possible carrier gas) and the number of surface reactions K equals 1.

Numerical solution method.—The above set of partial differential equations with boundary conditions is solved in two-dimensional, axisymmetric (r, z) form, using a control volume-based finite volume method (43). The equations are discretized on a non-uniform, cylindrical grid, which is shown in Fig. 2. It consists of 38 grid cells in the radial and 53 grid cells in the axial direction. Due to the particular geometry, *ca.* 80% of the grid cells are used for the computations. To check the grid independence of the results, calculations were also made on a 55 × 70 and a 70 × 90 grid for one representative situation. The calculated deposition rates obtained on these fine grids differed less than 0.1% from those obtained on the standard grid. For the discretization the so-called hybrid difference scheme (43) was used, which is an upwind scheme for high and a central scheme for low cell Peclet numbers, with the cell Peclet number a Peclet number based on the grid cell size. For our situations, because of the fine grid and low Reynolds numbers, a central difference scheme resulted in almost all grid cells in all cases.

The continuity equation was coupled to the momentum equation through a pressure correction method [SIMPLE (43)]. The equations were solved iteratively. Iteration is needed because of the nonlinearity of the equations, the coupling between the equations, and the use of non-direct, iterative solvers. Figure 3 gives a schematic representation of the solution procedure. Each solution step in the diagram of Fig. 3 corresponds to 2-6 solution sweeps, in which the equations are solved with a line by line method [TDMA, (43)] on horizontal or vertical lines, sweeping from top to bottom or vice versa, and from left to right or vice versa, respectively. As convergence criteria, the error in the global mass balance for the total flow ($<10^{-3}$%), the error in the global mass balance for each of the gas species (<0.1%), and the residuals of the equations (absolute values, summed over the grid, normalized by a characteristic value for the variable and normalized by the number of grid points, $<10^{-5}$), were used. Negligible changes in the calculated deposition rates occurred when more severe convergence criteria were used. The relative change from one iteration to the next in one particular monitor grid point and for each dependent variable has also been checked, and was typically less than 10^{-5}. All calculations were carried out on a HP 9000-560 minicomputer. To reach a fully converged solution, 1000-5000 iterations were needed, taking 12-60h of CPU time for one case.

Results

The mathematical model described in the previous sections was used to model the deposition of polysilicon from silane in a single wafer LPCVD reactor of the impinging jet type, shown in Fig. 1. The modeling was aimed at two purposes. The first was to evalute the importance of some physical phenomena in single wafer LPCVD. Thus, some insight is obtained into the question of how detailed a mathematical model for the transport phenomena in single wafer LPCVD should be. Second, the model was meant to evaluate a series of parameter variations, both in reactor geometry and in process conditions. In this way the model could be used as an aid in designing single wafer LPCVD reactors.

Evaluation of some modeling aspects in single wafer LPCVD.—The model described in the previous sections includes three aspects, often neglected in the modeling of either atmospheric pressure CVD or LPCVD in boat reactors, which may be important in single wafer LPCVD. In this section their relevance is discussed. For all cases described in this section, the radius of the inflow pipe R_p and the axial distance from the wafer surface to the end of the inflow pipe Z_p are 0.025m, the total flow rate Q is 0.2 slm, the silane mole fraction at the inlet is 0.1, and the wall and inflow temperatures T_w and T_{in} are 290 K. Also, for all cases in this section, the total pressure P_{tot} and wafer temperature T_h are 1 torr and 1000 K, respectively, thus following the tendencies in single wafer LPCVD to increase both pressure and temperature compared to conventional LPCVD in order to increase the growth rate.

Species balance coupling.—The dependence of the flow on the species balance equations is considered. In atmospheric pressure CVD, with highly diluted reactants and reaction products, this dependence is usually very small, thus allowing the sequential solution of the flow and species balance equations. The latter approach reduces the complexity of the problem and the computer time needed. Moreover, one flow field can be used as input for different concentration-reaction conditions (13, 24). In LPCVD however, reactants and reaction product concentrations can be high as well as their variations within the reactor. This causes large variations in the fluid properties. Furthermore, due to the deposition of solid species from gaseous reactants and the production of gaseous reaction products, there will be a change in the total volume flow through the reactor. Together, these effects cause the flow equations to be coupled to the species balance equations. To investigate the importance of this coupling, one particular situation was modeled using both the sequential solution approach and the fully coupled one.

In Fig. 4 the calculated deposition rates as a function of radius are shown, with hydrogen as carrier gas. Since it was assumed that the only gaseous reaction product is hydrogen (Eq. [29]), the gas mixture will consist of hydrogen and silane only in this case. Thus, Wilke's formulation for the diffusion fluxes (Eq. [13, 14]) could be used, which is identical to Fick's law of diffusion in binary gas mixtures. Line 1 represents a case in which the flow equations were solved first, evaluating the fluid properties at the inflow concentrations, followed by the solution of the species balance equations. By comparing this case to the fully coupled solution (line 2) it can be seen that the decoupled approach is strongly in error in this case, predicting deposition rates that are *ca.* 15% too low. Moreover, the non-uniformity ΔG predicted in the decoupled approach is 9.7%, whereas the fully coupled solution gives ΔG = 4.4%, with

$$\Delta G = \left| 1 - \frac{\text{growth rate at the edge of the wafer}}{\text{growth rate at the center of the wafer}} \right| \cdot 100\% \quad [31]$$

Aside from the fact that the species concentrations influence the flow equations through the fluid properties, there is a second important error in the decoupled approach. It is illustrated in Fig. 5, showing the streamlines of the mean gas flow as calculated in the fully coupled approach. Due to the high deposition rate, a large fraction of the incoming mass is deposited on the wafer, leading to a mass-averaged velocity component v_z into the wafer surface (Eq. [28]). In the decoupled approach this velocity will be zero, thus decreasing the reactants' supply to the wafer. It may therefore be concluded that the coupling of the flow equations to the species concentrations and surface reactions plays a significant role in single wafer LPCVD and cannot be neglected in single wafer LPCVD modeling.

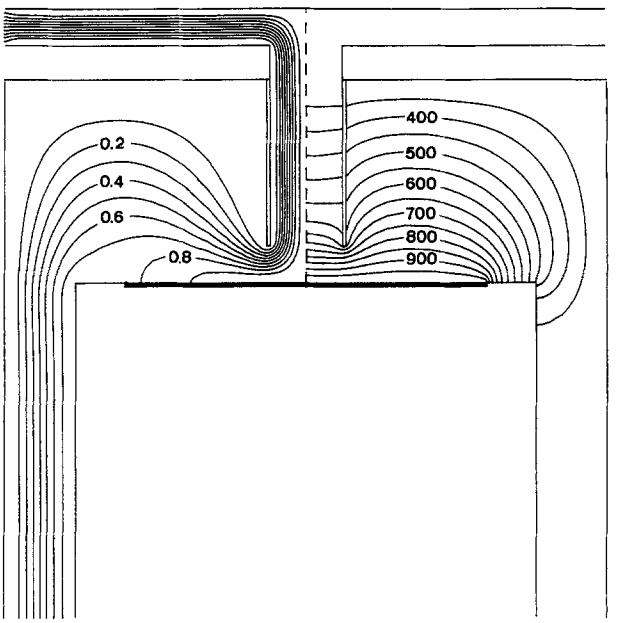

Fig. 5. Calculated streamlines (left) and isotherms (right) for case 2 of Fig. 4. Streamline values are normalized at the incoming mass flow.

Thermodiffusion.—The importance of thermodiffusion effects in single wafer LPCVD is investigated. In both cases described above, thermodiffusion was neglected. This can be done in hot wall LPCVD boat reactors. However, in cold wall atmospheric pressure systems, the influence of thermodiffusion was found to be significant (5, 10). Since single wafer LPCVD systems will usually have cooled walls, thermodiffusion is expected to play an important role in these reactors, too. Line 3 in Fig. 4 was obtained solving the coupled equations including thermodiffusion.

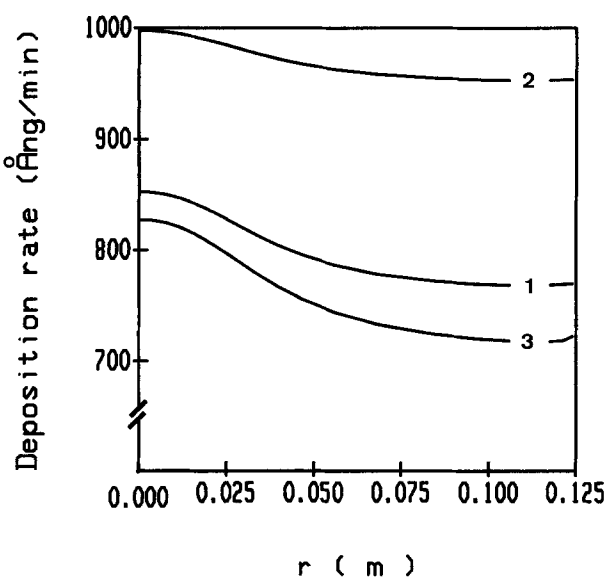

Fig. 4. Calculated deposition rate as a function of radius. P_{tot} = 1 torr, Q = 0.2 slm, T_h = 1000 K, Z_p = R_p = 0.025m. Incoming gas mixture: 90 mole percent (m/o) H_2 and 10 m/o SiH_4. 1: Decoupled flow and concentration equations, no thermodiffusion. 2: Coupled equations, no thermodiffusion. 3: Coupled equations, including thermodiffusion.

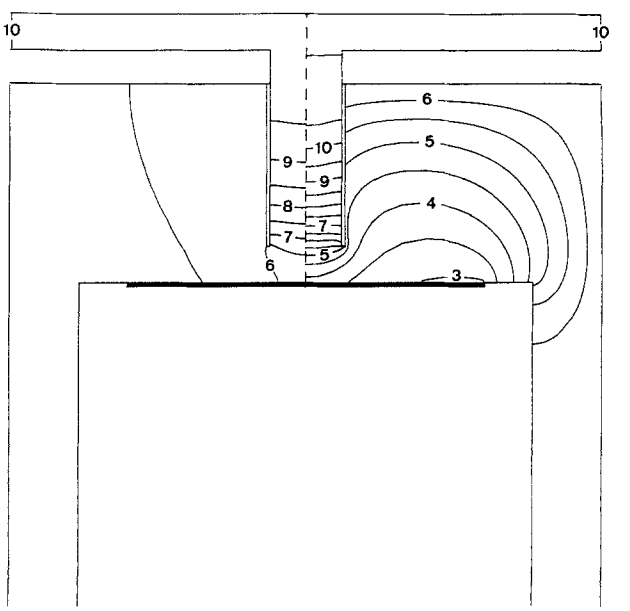

Fig. 6. Calculated contours for the silane mole fraction. Left: without thermodiffusion (Fig. 4, case 2). Right: with thermodiffusion (Fig. 4, case 3). Indicated values are mole fractions, $SiH_4 \cdot 10^2$.

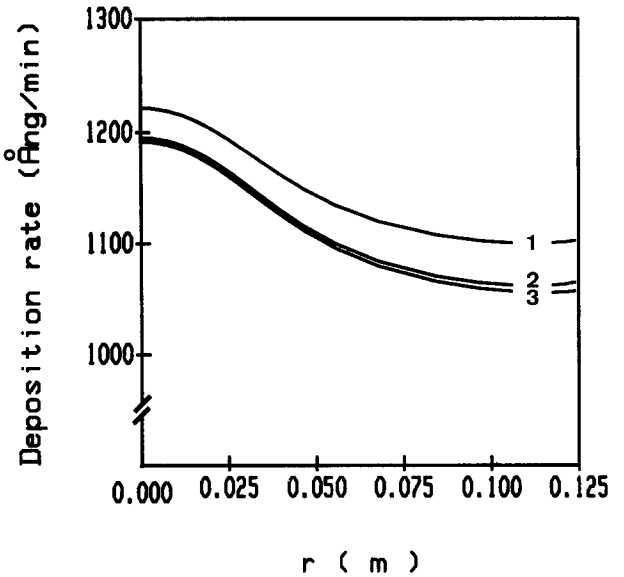

Fig. 7. Calculated deposition rate as a function of radius. P_{tot} = 1 torr, Q = 0.2 slm, T_h = 1000 K, Z_p = R_p = 0.025m. Incoming gas mixture: 90 m/o N_2 and 10 m/o SiH_4. 1: Wilke's approximation, no thermodiffusion. 2: Wilke's approximation, with thermodiffusion. 3: Stefan-Maxwell equations, with thermodiffusion.

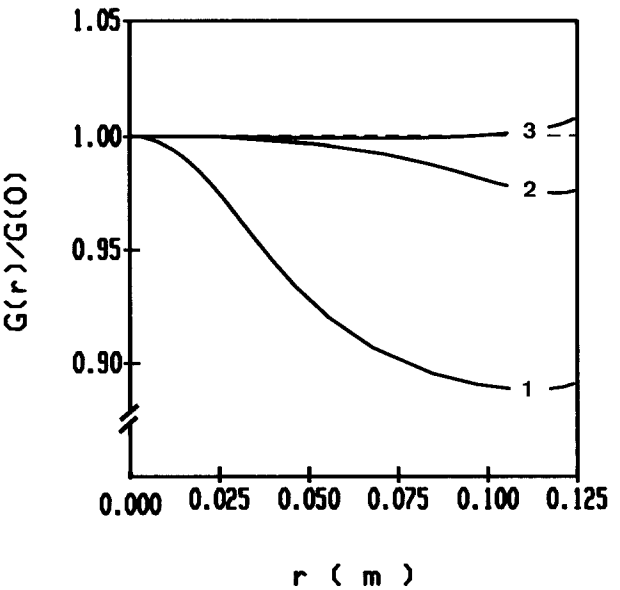

Fig. 9. The influence of the radius and the length of the inflow pipe on the growth uniformity. 1: Z_p = R_p = 0.025m. 2: Z_p = 0.025m, R_p = 0.10m. 3: Z_p = R_p = 0.10m. All other parameters as in Fig. 7.

Due to thermodiffusion, the large and heavy silane molecules are driven away from the heated susceptor, resulting in a decrease in the deposition rate by *ca.* 20%. Also, the growth non-uniformity is increased. This is due to the non-uniformity of the thermal boundary layer (Fig. 5) and the dramatic change in the concentration distribution caused by thermodiffusion (Fig. 6). It can be seen that silane is now concentrated in the cold upper parts of the reactor, even causing a local concentration maximum in the inflow pipe exceeding the inlet concentration. Since the differences in molecular weight and size between nitrogen and silane molecules are small, thermodiffusion has less influence when nitrogen is used as a carrier gas. This is shown in Fig. 7. Due to thermodiffusion, the growth rate is reduced only slightly in this case. From the above it may be concluded that thermodiffusion effects in single wafer LPCVD can be very important, depending on the combination of carrier gas and reactant. A general mathematical model for single wafer LPCVD should therefore include these effects.

Multicomponent mixture.—The accuracy of Wilke's approximation of multicomponent diffusion, compared to the exact Stefan-Maxwell equations, is studied. In the previous case, the incoming gas mixture consisted of nitrogen and silane, whereas hydrogen is formed in the surface reaction. Therefore, we have a three-component mixture, and Wilke's approximation is no longer fully correct. By comparing case 2 (computed using Wilke's approximation in which the silane and hydrogen concentrations were calculated from Eq. [5], [13], and [15], and the nitrogen concentration from Eq. [7]) and case 3 (computed using the Stefan-Maxwell equations) in Fig. 7 it can be seen that Wilke's approximation is accurate enough for all practical purposes in this case. This was to be expected, since both the silane and the hydrogen mass fractions are small in this case.

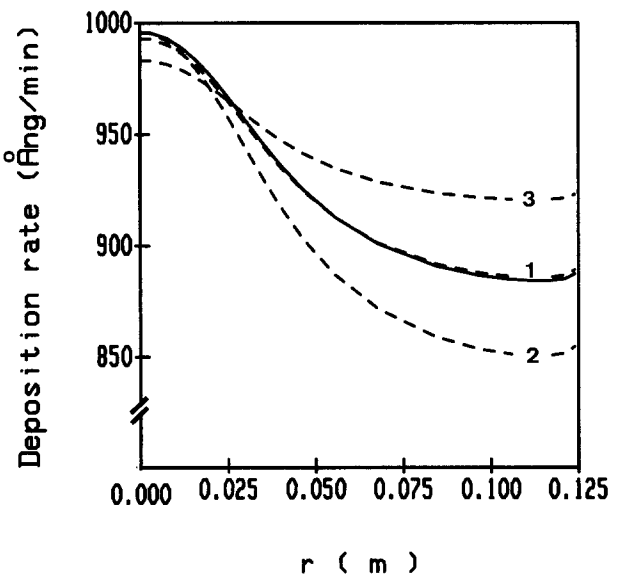

Fig. 8. Calculated deposition rate as a function of radius. P_{tot} = 1 torr, Q = 0.2 slm, T_h = 1000 K, Z_p = R_p = 0.025m. Incoming gas mixture: 45 m/o N_2, 45 m/o H_2, and 10 m/o SiH_4. 1: Wilke's approximation, N_2 from Eq. [7]. 2: Wilke's approximation, H_2 from Eq. [7]. 3: Wilke's approximation, SiH_4 from Eq. [7]. Continuous line: Stefan-Maxwell equations.

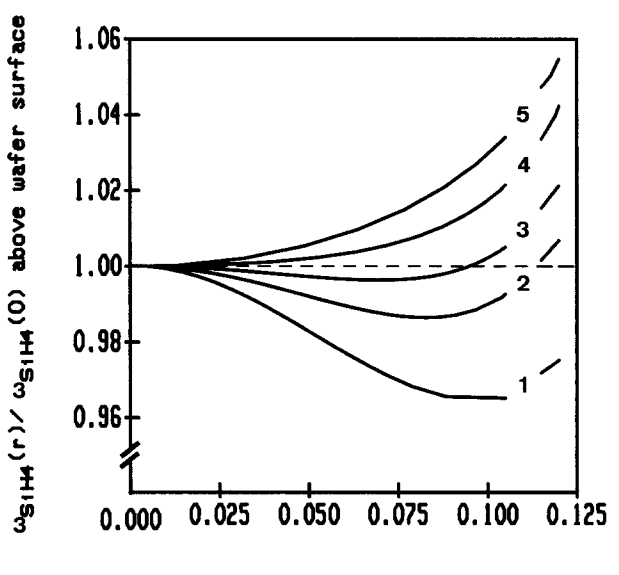

Fig. 10. Influence of variations in R_p on the radial variation in the silane concentration above the wafer surface. 1: R_p = 0.06m, 2: R_p = 0.08m, 3: R_p = 0.10m, 4: R_p = 0.12m, 5: R_p = 0.14m. All other parameters as in the base case.

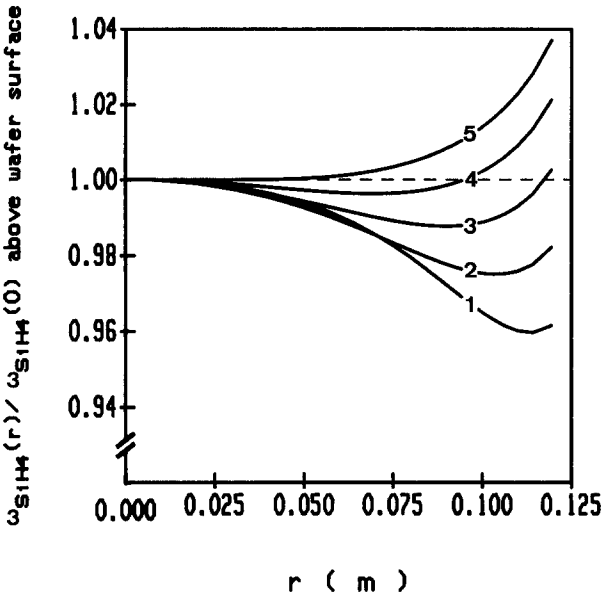

Fig. 11. Influence of variations in Z_p on the radial variation in the silane concentration above the wafer surface. 1: Z_p = 0.04m, 2: Z_p = 0.06m, 3: Z_p = 0.08m, 4: Z_p = 0.10m, 5: Z_p = 0.12m. All other parameters as in the base case.

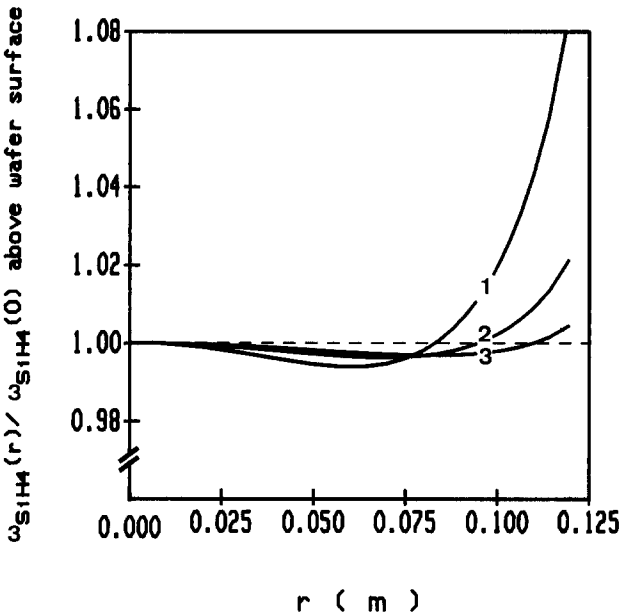

Fig. 13. Influence of the silane inflow mole fraction on the uniformity. 1: x_{in} = 0.05, 2: x_{in} = 0.10, 3: x_{in} = 0.20. All other parameters as in the base case.

A further look was taken at the accuracy of Wilke's approximation by modeling a situation in which an equimolal mixture of hydrogen and nitrogen was used as a carrier gas. In this case none of the species is present in great excess, so, when using Wilke's approximation, it is not clear which species should be calculated from Eq. [5], [13], [15], and which one from Eq. [7]. Therefore, all three possibilities were investigated. In Fig. 8 the calculated growth rates are shown. The non-uniformity can be seen to depend heavily on the way in which the species balance equations are solved. Thus, Wilke's approximation does not seem very reliable for this situation. When calculating the full Stefan-Maxwell equations for this same situation (Fig. 8, continuous line), growth rates are found that are very close to those obtained from Wilke's approximation, calculating the nitrogen concentration indirectly from Eq. [7].

From the above it may be concluded that a model for single wafer LPCVD should include coupling of the flow equations to the species balance equations, as well as thermodiffusion effects, in order to give accurate predictions of the growth rates. Multicomponent diffusion can be approximated accurately by Eq. [13] and [14] in many cases. However, when there is no carrier gas present in great excess, this approximation is ambigous and may lead to erroneous results. When using this approximation, it seems most favorable to use the additional Eq. [7] to calculate that species which is present in the largest mass fraction.

Parameter variations.—In all situations presented above, the growth non-uniformity was too large to meet present standards in the IC industry. Single wafer CVD reactors will have to produce layers that have a uniform thickness within 2-3%. Therefore, in this section, a series of parameter variations is investigated, both in reactor geometry and in process conditions, in order to optimize the deposition uniformity. In all cases, nitrogen was used as a carrier gas, since, as was shown in the previous section, higher growth rates and more uniform depositions are obtained in nitrogen than in hydrogen. Also, in all cases, the

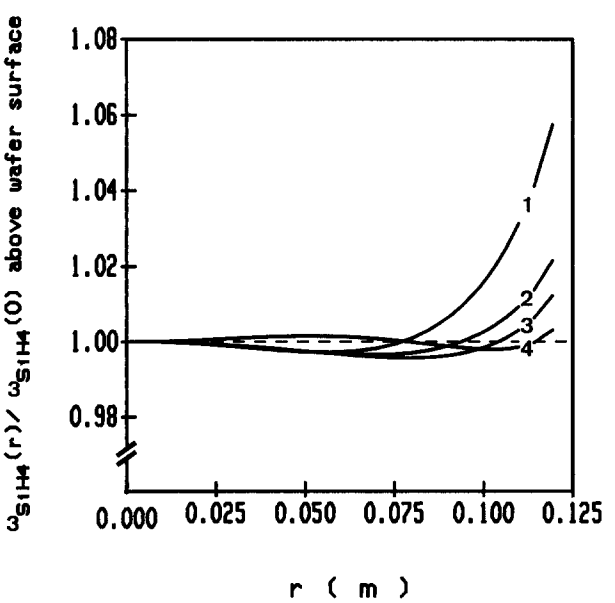

Fig. 12. Influence of the total flow rate, Q, on the uniformity. 1: Q = 0.3 slm, 2: Q = 1.0 slm, 3: Q = 3.0 slm, 4: Q = 10 slm. All other parameters as in the base case.

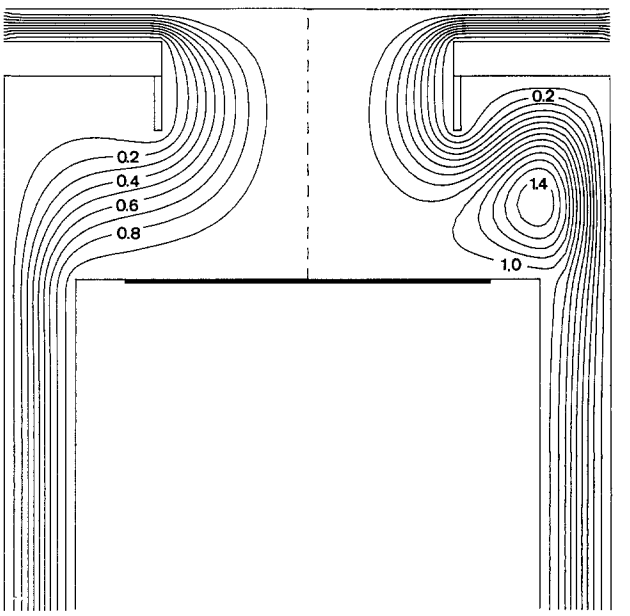

Fig. 14. Calculated streamlines (normalized at the incoming mass flow) for P_{tot} = 1 torr (left) and P_{tot} = 10 torr (right). All other parameters as in the base case.

Table III. Occurrence of buoyancy-induced recirculations

	P_{tot} (torr)		0.10	0.30	1.0	3.0	10
Q(slm)	Re	Gr	0.18	1.6	18	160	1800
0.30	1.1		–	–	–	+	+
1.0	3.5		–	–	–	–	+
3.0	11		–	–		–	+

coupling of the flow to the species concentrations was taken into account and thermodiffusion was included, since these effects were shown to have significant influence on the predicted growth rates. Finally, in all cases, we used Wilke's approximation for the multicomponent diffusion, since this approximation was shown to be very accurate when using nitrogen as a carrier gas and took less than half the computational time needed for the full Stefan-Maxwell equations.

Starting from the situation presented in Fig. 7 we started to vary the radius and length of the inflow pipe, in order to improve uniformity. The results are shown in Fig. 9. When the pipe radius R_p is increased from 0.025 to 0.10m, ΔG decreases from 10.5% to only 2.4%. A subsequent decrease of the length of the inflow pipe, thus increasing Z_p from 0.025 to 0.10m, further improves the uniformity, leading to $\Delta G = 0.7\%$. Thus it can be seen how minor changes in reactor design, which can easily be studied with the model developed, may lead to significant improvement in layer uniformity.

A further study of the influence of parameter variations, both in reactor geometry and in process conditions, was made to obtain a deeper insight in the effects of these variations on growth uniformity. In this parameter variation study we used a slightly different approach. Instead of calculating the deposition rate from Eq. [30], we used a fixed, uniform deposition rate of 2000 Å/min, thus replacing Eq. [30] by

$$R = 2.73 \cdot 10^{-4}\ \text{mol} \cdot m^{-2} \cdot s^{-1} \rightarrow G = 2000\ \text{Å} \cdot \text{min}^{-1}$$

Such a high growth rate will be needed to obtain sufficient throughput in single wafer LPCVD. Using this uniform deposition rate, we looked at the radial variation of the silane mass fraction in the first grid cells (*i.e.*, 1 mm) above the wafer surface. In order to actually obtain uniform deposition, the reactants' concentration should be uniform over the wafer surface. By using this approach, the results are no longer strictly limited to the deposition of silicon from silane through Eq. [30], but can more generally be

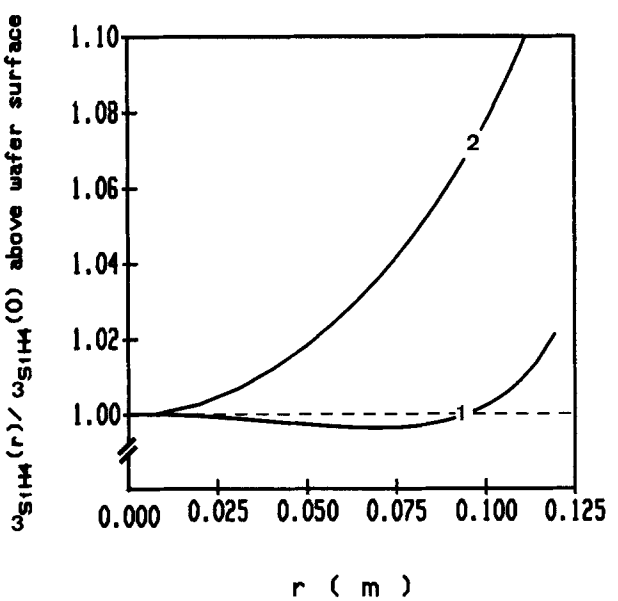

Fig. 15. Influence of recirculation on uniformity. 1: No recirculation (P_{tot} = 1 torr), 2: strong recirculation (P_{tot} = 10 torr). All other parameters as in the base case.

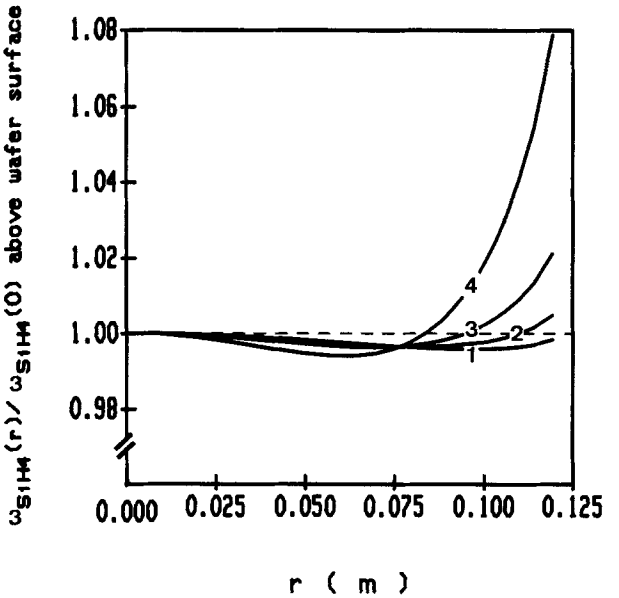

Fig. 16. Influence of the growth rate on the uniformity. 1: G = 500Å/min, 2: G = 1000 Å/min, 3: G = 2000 Å/min, 4: G = 4000 Å/min. All other parameters as in the base case.

used to obtain insight in the influence of several parameters on growth uniformity.

Starting from a base case, we varied the radius and length of the inflow pipe, the total flow rate, the inlet concentration of silane, the total pressure, and the deposition rate, one by one. In the base case we used the following set of parameters: $R_p = Z_p = 0.10\ m$, $Q = 1$ slm, inlet mole fraction silane = 0.10, $P_{tot} = 1$ torr, $G = 2000$ Å/min, $T_w = T_{in} = 290$ K, $T_h = 900$ K, N_2 carrier gas.

In Fig. 10 and 11 the influence of R_p and Z_p on the silane concentration uniformity above the wafer is shown. Again it can be seen that these two parameters offer an easy way for tuning the uniformity. When R_p and Z_p are increased, a stagnation point flow situation is approached, whereas for small R_p and Z_p the configuration is more like a real impinging jet. Indeed, in the first case we find higher silane concentrations at the wafer edge, which agrees with modeling results for stagnation point flow configurations (22-24). In the latter case the maximum is found in the center.

In Fig. 12 the influence of the total flow rate on the uniformity is shown. As was clearly to be expected, uniformity is improved when the total flow rate is increased, keeping the silane concentration fixed. However, by doing so, the silane is used less efficiently. One could also increase the silane supply by increasing its inlet concentration, keeping the flow rate fixed. This is illustrated in Fig. 13. Again, at a higher reactant supply, uniformity is improved. However, by tripling the total flow rate at fixed silane concentration, less improvement is obtained than by doubling the silane input concentration at fixed total flow rate. Thus, the latter approach seems clearly favorable, provided the silane partial pressure is kept low enough to prevent gas phase nucleation.

When the total pressure in increased, the danger occurs that buoyancy effects will become significant, creating recirculating flows in the reactor, especially when nitrogen is used as a carrier gas. In Fig. 14 calculated streamlines are shown for total pressures of 1 and 10 torr. Strong recirculation is created at $P_{tot} = 10$ torr, causing serious nonuniformity (Fig. 15). Moreover, the importance of such a recirculating flow, acting as a memory cell when the reactant supply is turned off, has been indicated by Opdorp and Leys (44). Its appearance was found to depend on the value of a mixed convection parameter Gr/Re^k, with $1 \leq k \leq 2$ (20, 45). To prevent recirculating flow one should increase the Reynolds number Re or decrease the Grashof number Gr. For a particular reactor geometry, wafer temperature and gas mixture, Re is a function of the flow rate only,

whereas Gr is a function of the pressure only. Thus, recirculating flows may be suppressed by increasing the flow rate or decreasing the total pressure. In Table III an overview is given of the appearance of recirculating flows in the present reactor, using nitrogen as a carrier gas. Finally, in Fig. 16, the influence of the growth rate on the uniformity is shown. As was to be expected, uniformity decreases at higher deposition rates.

Conclusion

A mathematical model has been developed for LPCVD in a single wafer reactor of the impinging jet type. It was shown that such a model should combine an accurate description of phenomena that up to now were taken into account in the modeling of atmospheric pressure cold wall CVD systems only (such as complex gas flow and thermodiffusion) and of phenomena that are relevant in conventional LPCVD (such as multicomponent diffusion and coupling of flow equations to the species balance equations). The model incorporates both the Stefan-Maxwell equations and an approximate expression derived by Wilke (32) for multicomponent diffusion. The latter approach takes much less computing time, giving accurate predictions in many cases. However, when no gas is present in great (mass fraction) excess, this approach becomes unreliable. An improvement may possibly be obtained by applying a slightly different version of this approximation, described by Coffee and Heimerl (33), in which the error caused by the approximation is equally divided over all species, instead of concentrating it in just one species. This is a topic of present research.

By using the model in a parameter variation study, varying both reactor geometry and process conditions, the model could be used as an aid to design a single wafer reactor in which high deposition uniformities (within 2-3%) can be reached on large wafers (0.25m diameter) at high growth rates (2000 Å/min). This uniformity could be reached by a simple optimization of the geometric configuration, as well as by making appropriate changes in the process conditions (such as total flow rate, reactant concentration, and total pressure). Finally, it was shown that at high pressures (3-10 torr) buoyancy-induced return flows may occur when nitrogen is used as a carrier gas. This effect may be suppressed by a sufficient increase in the total flow rate.

Acknowledgments

This work forms part of the research program of the "Stichting Fundamenteel Onderzoek der Materie" (Foundation for Fundamental Research of Matter—FOM) and of the "Innovatief Onderzoeks Programma IC technologie" (Innovating Research Program for IC Technology), and was made possible by the financial support from the "Nederlandse Organisatie voor Zuiver Wetenschappelijk Onderzoek" (The Netherlands Organization for the Advancement of Pure Research—ZWO) and from the Dutch Ministry of Economic affairs.

Manuscript submitted Nov. 21, 1988; revised manuscript received April 24, 1989.

Delft University of Technology assisted in meeting the publication costs of this article.

LIST OF SYMBOLS

c	total mole concentration, mol · m^{-3}
c_p	specific heat, J · kg^{-1} · K^{-1}
D	binary diffusion coefficient, m^2 · s^{-1}
$\mathbb{D}$	effective diffusion coefficient, m^2 · s^{-1}
$\mathbb{D}'$	effective diff. coeff. according to Wilke, m^2 · s^{-1}
$\mathbb{D}^T$	multicomponent thermodiffusion coefficient, kg · m^{-1} · s^{-1}
$\mathbf{g}$	gravity vector, N · kg^{-1}
G	growth rate, Å · min^{-1}
ΔG	non-uniformity in the growth rate
Gr	Grashof number $\mathbf{g}\rho^2_{ref} H^3 (T_h - T_w)/(\mu^2_{ref} T_{ref})$
H	distance from wafer to upper wall reactor, m
$\mathbf{I}$	unity tensor
$\mathbf{j}$	diffusive mass flux vector, kg · m^{-2} · s^{-1}
$\mathbf{J}$	diffusive mole flux vector, mol · m^{-2} · s^{-1}
k	thermodiffusion ratio
k	constant in the rate expression for the surface reaction, mol · m^{-2} · s^{-1} · Pa^{-1}
K	total number of surface reactions
K_H	constant in the rate expression for the surface reaction, Pa$^{-1/2}$
K_S	constant in the rate expression for the surface reaction, Pa^{-1}
m	averaged mole mass, kg · mol^{-1}
m_i	mole mass of species i, kg · mol^{-1}
M	total mass deposition rate on the wafer, kg · m^{-2} · s^{-1}
M_i	total mass deposition rate of species i on the wafer, kg · m^{-2} · s^{-1}
N	total number of gaseous species
P	pressure, N · m^{-2}
P_{tot}	total pressure in the outlet of the reactor, N · m^{-2}
Q	total flow rate, slm
R	universal gas constant, J · mole^{-1} · K^{-1}
R_p	radius of the inflow pipe, m
R_k	reaction rate of kth surface reaction, mol · m^{-2} · s^{-1}
Re	Reynolds number $\rho_{ref} V_P R_P/\mu_{ref}$
S	total number of solid species participating in surface reactions
T	temperature, K
$\mathbf{v}$	mass averaged velocity vector, m · s^{-1}
V_P	average velocity in the inflow pipe, m · s^{-1}
x	mole fraction
Z_p	axial distance from the wafer surface to the end of the inflow pipe, m

Greek Symbols

γ_{ik}	stoichiometric coefficient for gaseous species i in surface reaction k
κ	volume viscosity, kg · m^{-1} · s^{-1}
λ	thermal conductivity, W · m^{-1} · K^{-1}
μ	dynamic viscosity, kg · m^{-1} · s^{-1}
ρ	density of the gas mixture, kg · m^{-3}
σ_{jk}	stoichiometric coefficient for solid species j in surface reaction k
τ	viscous stress tensor, N · m^{-2}
ω	mass fraction

Superscripts

T	transposed
T	due to thermal diffusion
c	due to ordinary (concentration) diffusion

Subscripts

h	at the heated wafer surface
i, j	with regard to a specific gas species i or j
ij	with regard to the binary gas pair i and j
in	in the inlet of the reactor
r	radial component of a vector
ref	at the reference temperature $0.5 \cdot (T_h + T_w)$
w	at the reactor walls
z	axial component of a vector

REFERENCES

1. A. Sherman, "Chemical Vapor Deposition For Microelectronics," Noyes Publications, New Jersey (1987).
2. W. H. Shepherd, *This Journal*, **112,** 988 (1965).
3. F. C. Eversteijn, P. J. W. Severin, C. H. J. van den Brekel, and H. L. Peek, *ibid.*, **117,** 925 (1970).
4. M. E. Coltrin, R. J. Kee, and J. A. Miller, *ibid.*, **131,** 425 (1984).
5. M. E. Coltrin, R. J. Kee, and J. A. Miller, *ibid.*, **133,** 1206 (1986).
6. W. G. Breiland, M. E. Coltrin, and P. Ho, *J. Appl. Phys.*, **59,** 3267 (1986).
7. W. G. Breiland, M. E. Coltrin, and P. Ho, *ibid.*, **60,** 1505 (1986).
8. W. G. Breiland, P. Ho, and M. E. Coltrin, in "Chemical Vapor Deposition 1987," G. W. Cullen, Editor, p. 912, The Electrochemical Society Softbound Proceedings Series, Vol. 87-8, Pennington, NJ (1987).
9. J. van de Ven, G. J. M. Rutten, M. J. Raaymakers, and L. J. Giling, *J. Cryst. Growth*, **76,** 352 (1986).
10. J. Ouazzani, K. Chiu, and F. Rosenberger, *ibid.*, **91,** 497 (1988).
11. H. Moffat and K. F. Jensen, *ibid.*, **77,** 108 (1986).
12. J. Jůza and J. Cérmak, *This Journal*, **129,** 1627 (1982).
13. H. Moffat and K. F. Jensen, *ibid.*, **135,** 459 (1988).
14. K. F. Jensen and D. B. Graves, *ibid.*, **130,** 1950 (1983).

15. K. F. Roenigk and K. F. Jensen, *ibid.*, **132,** 448 (1985).
16. D. W. Hess, K. F. Jensen, and T. J. Anderson, *Reviews in Chem. Engineering,* **3,** 97 (1985).
17. K. F. Jensen, *Chem. Eng. Sci.,* **42,** 923 (1987).
18. K. F. Jensen, in "Chemical Vapor Deposition 1984," McD. Robinson *et al.,* Editors, p. 3, The Electrochemical Society Softbound Proceedings Series, Vol. 84-6, Pennington, NJ (1984).
19. R. Pollard and J. Newman, *This Journal,* **127,** 744 (1980).
20. G. Evans and R. Greif, *Num. Heat Transfer,* **12,** 243 (1987).
21. G. Evans and R. Greif, *J. Heat Transfer,* **109,** 928 (1987).
22. G. Wahl, *Thin Solid Films,* **40,** 13 (1977).
23. G. Wahl, in "Chemical Vapor Deposition 1984," McD. Robinson *et al.,* Editors, p. 60, The Electrochemical Society Softbound Proceedings Series, Vol. 84-6, Pennington, NJ (1984).
24. C. Houtman, D. B. Graves, and K. F. Jensen, *This Journal,* **133,** 961 (1986).
25. P. Lee, D. McKenna, D. Kapur, and K. F. Jensen, *J. Cryst. Growth,* **77,** 120 (1986).
26. M. Michaelidis and R. Pollard, *This Journal,* **131,** 860 (1984).
27. J. P. Jenkinson and R. Pollard, *ibid.,* **131,** 2911 (1984).
28. H. Tennekes and J. L. Lumley, "A First Course in Turbulence," MIT Press, Cambridge, Mass. (1983).
29. R. Krishnamurti, *J. Fluid Mechanics,* **60,** 285 (1973).
30. K. Chiu, J. Ouazzani, and F. Rosenberger, *Int. J. Heat Mass Transfer,* **30,** 1645 (1987).
31. R. B. Bird, W. E. Stewart, and E. N. Lightfoot, "Transport Phenomena," pp. 79, 570, J. Wiley & Sons, New York (1960).
32. C. R. Wilke, *Chem. Eng. Prog.,* **46,** 95 (1950).
33. T. P. Coffee and J. M. Heimerl, *Combust. Flame,* **43,** 273 (1981).
34. R. Svehla, NASA Technical Report R-132, Ohio (1962).
35. J. O. Hirschfelder, C. F. Curtiss, and R. B. Bird, "Molecular Theory of Gases and Liquids," pp. 541, 543, J. Wiley & Sons, New York (1954).
36. G. C. Maitland and E. B. Smith, *J. Chem. Eng. Data,* **17,** 150, (1972).
37. l'Air Liquide, Division Scientifique, "Encyclopedie des Gaz," Elsevier Scientific Publ. Co., Amsterdam (1976).
38. "Handbook of Chemistry and Physics," R. C. Weast, Editor, CRC Press, Florida (1980).
39. S. Bretsznajder (translated by J. Bandrowski), "Prediction of Transport and Other Physical Properties of Fluids," Pergamon Press, Oxford (1971).
40. R. Clark Jones, *Phys. Rev.,* **59,** 1019 (1941).
41. M. L. Hitchman, J. Kane, and A. E. Widmer, *Thin Solid Films,* **59,** 231 (1979).
42. B. S. Meyerson and W. Olbricht, *This Journal,* **131,** 2361 (1984).
43. S. V. Patankar, "Numerical Heat Transfer and Fluid Flow," McGraw-Hill Book Company, New York (1980).
44. C. van Opdorp and M. R. Leys, *J. Cryst. Growth,* **84,** 271 (1987).
45. E. P. Visser, C. R. Kleijn, C. A. M. Govers, C. J. Hoogendoorn, and L. J. Giling, *ibid.,* **94,** 929 (1989); **96,** 732 (1989).

Stress Measurements of Thermally Grown Thin Oxides on (100) Si Substrates

L. M. Mack and A. Reisman*

Microelectronics Center of North Carolina, Research Triangle Park, North Carolina 27709
and
North Carolina State University, Department of Electrical and Computer Engineering, Raleigh, North Carolina 27965

P. K. Bhattacharya

Microelectronics Center of North Carolina, Research Triangle Park, North Carolina 27709

ABSTRACT

The results of film stress measurements on thermally oxidized silicon substrates are presented and discussed. The oxides were grown to thicknesses ranging between 9.0 and 37.0 nm at 800°-1000°C in dry O_2 with 4.5% HCl at atmospheric pressure on double-side polished, 100 μm, 0.5 and 0.1 Ω-cm, p-type (100) Si wafers. The oxide film stress was determined through curvature measurements using a single beam laser reflection technique, which is described. The total compressive film stress, as measured at room temperature, was on the order of -5×10^9 dyne/cm^2. The intrinsic film stress, *i.e.,* the total stress less the thermal coefficient of expansion stress, was found not to depend on the thickness of the oxide grown at a given oxidation temperature in the thickness range studied. The intrinsic stress decreased linearly with increasing oxidation temperature for oxides of similar thickness. It was found that the total oxide film stress was the same for samples grown on 0.5 Ω-cm and 0.1 Ω-cm substrates. Comparisons of curvature measurements of the bare Si wafers before processing and after removal of the grown oxide occasionally showed the occurrence of plastic deformation of the substrates during the oxidation process. The effects of this plastic deformation are considered.

Thermal oxidation of silicon substrates is an integral part of the fabrication process of insulated gate field effect transistors (IGFETs). Control of the growth of the gate dielectric represents a particularly critical step in the process, since variations in the thickness of the gate dielectric can have a pronounced effect upon the IGFET threshold voltage. Therefore, control of the gate oxidation process is of importance in the manufacture of VLSI circuits, where gate oxide thicknesses are of the order of several hundred angstroms today, and are expected to decrease to about 12.5 nm in 0.5 μm groundrule IGFETs. Unfortunately, the growth of thin oxides is not well understood, and until recently (1) a model which accurately describes the oxidation kinetics has not been available. To date, control of gate oxide growth has been achieved using low oxidation temperatures where growth rates are very low. But gate oxide growth at elevated temperatures is postulated as offering advantages, such as reduced oxide defect levels and lower oxide film stress (2-6).

It has been proposed that an intrinsic oxide film stress develops due to the 120% molar volume expansion of SiO_2 over Si during oxidation (7). Oxide film stress, or viscosity variations with time may influence oxidation kinetics. Thus viscosity (8), or stress (10-13) dependent terms are included in a number of recently published oxidation models. Such models have been proposed to explain the growth kinetics of the so-called "anomalous" region of oxidation, and hence provide a physically based model which completely describes oxidation kinetics. In line with this, measurements of the oxide film stress of thin oxides may

* Electrochemical Society Active Member.